Journal of Materials Chemistry A

Accepted Manuscript

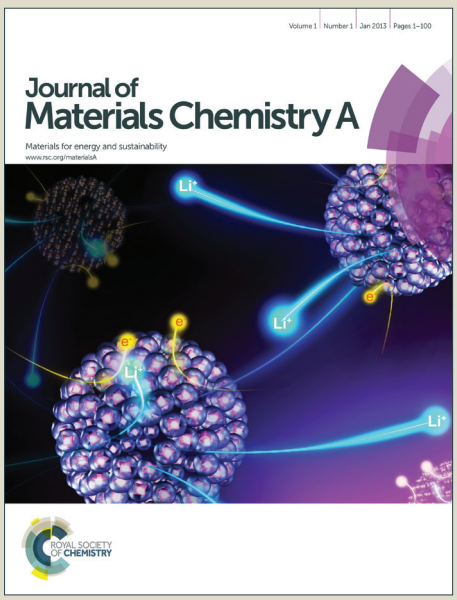

ROYAL SOCIETY OF CHEMISTRY

www.rsc.org/materialsA

Journal of Materials Chemistry A

ARTICLE

Nanoflower-like metallic conductive MoO_2 as a high-performance non-precious metal electrocatalyst for hydrogen evolution reaction

Received 00th January 20xx,
Accepted 00th January 20xx

DOI: 10.1039/x0xx00000x

www.rsc.org/

Yanshuo Jin,[a] and Pei Kang Shen*[,a]

Searching for hydrogen evolution reaction (HER) non-precious metal electrocatalysts with high activity and stability has attracted considerable attention. Herein, we report the synthesis of nanoflower-like MoO_2 on nickel foam (NFL MoO_2/NF). Remarkably, as a HER electrocatalyst operating in alkaline electrolyte, NFL MoO_2/NF exhibits high stability and activity. The onset potential of NFL MoO_2/NF is almost 0V versus the reversible hydrogen electrode (RHE) and bubbles can be produced on the surface of NFL MoO_2/NF under static overpotential of only 10 mV, comparable to commercial Pt/C. NFL MoO_2/NF needs overpotentials of only about 55 and 80 mV to achieve current densities of 10 and 20 mA cm^{-2}, respectively. NFL MoO_2/NF has superior stability in the long-term electrochemical process and keeps 94.3 percent of its initial current density after 25 hours.

Introduction

Hydrogen has been proposed as an alternative to the diminishing fossil fuel.[1] Electrolysis of water into hydrogen and oxygen in an electrolyzer is the simplest way to produce high-purity hydrogen.[2] Nickel (Ni) is typically used in industry for water electrolysis in alkaline solution but with high overpotential and large Tafel slope.[3] The platinum (Pt) and its alloys are the best HER catalysts, but the cost and scarcity of Pt are serious impediments to its large-scale industrial application for electrolysis.[4, 5] These disadvantages have motivated many research efforts and some active and stable non-precious metal-based HER catalysts have been pursued in the past few years.[6, 7] Molybdenum based non-precious-metal compounds have been intensively studied for HER catalysts, including MoS_2,[8-12] $MoSe_2$,[8, 13] MoB,[14] Mo_2C,[14-18] MoP[19, 20] and so on.

According to the literature data, molybdenum based metallic transition metal oxide MoO_2 crystallizes in a monoclinic cell and has a distorted rutile structure.[21] The banding is a complex and involves delocalization of some of the Mo electrons in a conductance band accounting for the metallic conductivity.[21] Tungsten based metallic transition metal oxide WO_2 has the same distorted rutile crystal structure with MoO_2 and exhibits excellent performance for H_2 generation: the onset overpotential is only 35 mV.[22] Thus, metallic transition metal oxide is a potential candidate of electrocatalyst for hydrogen evolution reaction.

Polymer binder (Nafion or PTFE) is usually used to immobilize the catalysts on electrode surface for electrochemical measurements and practical applications.[23] However, the whole process is time-consuming and the polymer binder may reduce effective catalytic activity because it blocks active sites and reduces gas permeability and increases mass transfer overpotential.[24] Thus, the problem can be solved by synthesizing eletrocatalystic nanomaterials on substrates without binder.[25]

Herein, we report on our recent efforts in developing a novel nanoflower-like MoO_2 on nickel foam (NF). The nanoflower-like $MoO_2{\cdot}2H_2O$ precursor was directly grown on commercial nickel foam (NFL $MoO_2{\cdot}2H_2O$/NF) by a wet-chemical route first. With an annealing treatment at 500 ^oC in N_2 atmosphere and a subsequent annealing treatment at 400 ^oC in H_2 atmosphere were used to synthesize NFL MoO_2/NF. As an integrated non-precious metal high-performance cathode for generating hydrogen from alkaline solution, the NFL MoO_2/NF maintains its activity for at least 50 hours and shows an onset potential of almost 0V, a Tafel slope of 66 mV dec^{-1}. NFL MoO_2/NF needs overpotential of only about 55 and 80 mV to achieve current densities of 10 and 20 mA cm^{-2}, respectively. The large exchange current density (~1.8 mA cm^{-2}) of NFL MoO_2/NF can be associated with its high surface area, corresponding many more active sites exposed for HER.

Experimental

Materials

Ammonium molybdate tetrahydrate ($(NH_4)_6Mo_7O_{24}{\cdot}4H_2O$), hydrochloric acid (HCl), potassium hydroxide (KOH) and Ni

[a] State Key Laboratory of Optoelectronic Materials and Technologies, School of Physics and Engineering, Sun Yat-sen University, Guangzhou, 510275, P. R. China. E-mail: stsspk@mail.sysu.edu.cn

† Electronic Supplementary Information (ESI) available: [details of any supplementary information available should be included here]. See DOI: 10.1039/x0xx00000x

foam were purchased from Dongzheng Ltd. All chemical reagents used in this experiment were of analytical grade. The water used throughout all experiments was purified through a Millipore system.

Synthesis of NFL $MoO_2 \cdot 2H_2O$/NF

Two Ni foams (40.0 mm×20.0 mm×1.0 mm) were cleaned by diluted hydrochloric acid, ethanol and deionized water for several times. Then, 20 mmol L^{-1} $(NH_4)_6Mo_7O_{24} \cdot 4H_2O$ were dissolved in 35 mL deionized water at room temperature to form a uniform solution. The solution was subsequently transferred into a 50 mL Teflon-lined stainless steel autoclave, and the pre-treated Ni foams were placed upright in the autoclave. The autoclave was heated to 100 °C in an electric oven and maintained for 18 h, after that the Ni foams with precursor were cleaned with deionized water for several times before being fully dried in air at 60 °C.

Synthesis of NFL MoO_2/NF

NFL $MoO_2 \cdot 2H_2O$ /NF was annealed in N_2 at 500 °C for 1 h and subsequently in H_2 at 400 °C for 1 h.

Synthesis of NFL $MoO_2(MoO_3)$/NF

NFL $MoO_2 \cdot 2H_2O$/NF was annealed in N_2 at 500 °C for 1 h.

Calculated MoO_2 loading

NFL MoO_2/NF was immersed in a 35 % HCl solution for one day, then was filtered, dried and weighed.

Characterizations

Powder XRD data were acquired on a D-MAX 2200 VPC diffractometer with Cu Ka radiation (λ=1.54056Å). The Raman spectrum was performed on a micro-Raman system (Renishaw, in via). IR spectrum was performed on a Nicolet6700/Thermo/America Fourier transform infrared spectrometry. DSC of the products was carried out on a DSC-204/Netzsch/Bruke differential scanning calorimetr. SEM measurements were carried out on a Quanta 400/INCA/HKL scanning electron microscope at an accelerating voltage of 30 kV. TEM measurements were performed on a Tecnai G2 F30 transmission electron microscope at 300 kV. XPS measurements were performed on an ESCALAB 250 system.

Electrochemical measurements

The electrochemical measurements were conducted in a typical three-electrode setup with a reversible hydrogen electrode (RHE) as the reference electrode and a graphite rod as the counter electrode. Steady-state potential polarization curves were measured in 1M KOH solution under different temperatures. Accelerated degradation measurement was conducted for 3000 cyclic voltammetry (CV) cycles in 1M KOH solution at a scan rate of 50 mV s^{-1} and linear sweep voltammetry (LSV) measurements were conducted at a scan rate of 1 mV s^{-1}. Electrochemical impedance spectra (EIS) experiments were performed with the three-electrode cell system in 1M KOH at 25 ^{o}C. The potentiost has a frequency range of 1 kHz-100 mHz in a 10.0 mV AC voltage.

Results and discussion

After hydrothermal treatment, nanoflower-like precursor is grown on the Ni foam which changes in color from silver-grey to reddish brown and then the color changes to black after annealing treatments (Figure S1, Supporting Informatioon). Figure 1a shows the X-ray diffraction (XRD) pattern of the NFL MoO_2/NF, the peaks which assigned to monoclinic MoO_2 (PDF#65-5787) were detected. The strong peaks at 44.5°, 51.8°, and 76.4° originate from to the Ni foam substrate (PDF#65-2865). Figure 1b shows the Raman spectrum, the monoclinic MoO_2 was detected with Raman bands at 200, 226, 345, 351, 456, 492, 569 and 739 cm^{-1}.[26]

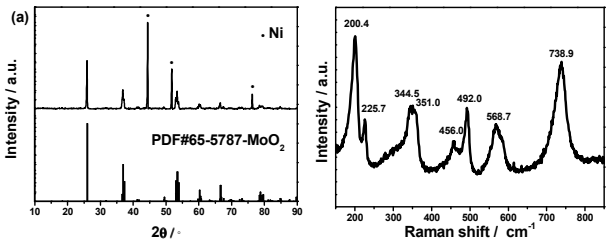

Fig. 1. a) XRD pattern and b) Raman spectrum of NFL MoO_2/NF.

Figure S2, Supporting Informatioon shows the scanning electron microscopy (SEM) images of nanoflower-like precursor/Ni foam, indicating that the entire surface of the Ni foam is uniformly covered by nanoflower-like/calyx-type precursor. IR spectrum of the precursor is consistent with the standard spectrum of the molybdenum dioxide. As shown in Figure S3a, Supporting Informatioon, the intense band at 950 cm^{-1} is assigned to *ν*(Mo=O), while the prominent bands in the range of 500-850 cm^{-1} are attributed to *ν*(Mo-O-Mo). In addition, the broad band at 3210 cm^{-1} and 1610 cm^{-1} correspond to the absorbed water.[27] Figure S3b shows the XRD pattern of the precursor, but it is still hard to judge what the precursor is. The TG and DTA curves of the precursor in N_2 atmosphere are shown in Figure S4, Supporting Informatioon. It shows two major events. The endothermic peak and exothermic peak at 121 °C and 485 °C on the DTA curve give two thermal behaviors. The broad endothermic peak on the DTA curve at about 121 °C corresponds to the release of the adsorbed water.[27] The sharp exothermic peak at 485 °C is associated with the formation of crystalline MoO_2 in N_2 atmosphere (Figure S5, Supporting Informatioon), it is the same as the data reported in literature.[27] The mass loss of 21 % is corresponding to the loss of almost two molecular absorbed water (theoretical value 22 %) and we can deduce that the precursor is $MoO_2 \cdot 2H_2O$. So we can conclude that the reaction mechanism is expressed by Equation (1) and Equation (2) in the hydrothermal synthesis reactor and the tube furnace, respectively.

$$20\ (NH_4)^+ + (Mo_7O_{24})^{6-} + 7\ Ni + 4\ H_2O \rightarrow 20\ NH_3\uparrow + 7\ MoO_2 \cdot 2H_2O + 7\ Ni^{2+} \quad (1)$$

$$MoO_2 \cdot 2H_2O \rightarrow MoO_2 + 2H_2O \quad (2)$$

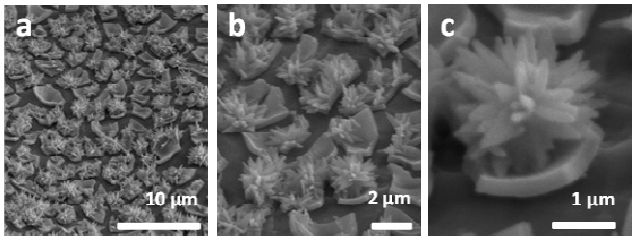

Fig. 2. a-c) SEM images with different magnifications of the NFL MoO_2/NF.

Scanning electron microscopy (SEM, Figure 2a,b) images of NFL MoO_2/NF show that the nanoflower-like morphology is preserved and the entire surface of the nickel foam is uniformly covered by nanoflower-like MoO_2. A close view of nanoflower-like MoO_2 (Figure 2c) reveals that nanoflower-like morphology is consisted of many nanosheets and the bulk MoO_2 plays a role in linking nanoflower-like MoO_2 and nickel foam. The nanoflower-like structure could lead to much higher surface area than bulk materials, so nanoflower-like structure contributed the majority of the active sites exposed for HER. The corresponding energy dispersive X-ray (EDX) spectrum (Figure S6, Supporting Informatioon) verifies the 1:2 atomic ratio of Mo to O. The skeletal structure of the Ni foam was maintained completely, thus enabling its direct use as an integrated three-dimensional cathode for HER. Transmission electron microscopy (TEM, Figure 3a) and high-resolution (HR) TEM (Figure 3b) images show that the nanoflower-like MoO_2 is consisted of many nanoparticles, forming lamellar superstructures at the micrometer scale. The HRTEM image shows well-resolved lattice fringes with an interplanar distance of 0.48 nm, which corresponds to the (100) plane of the MoO_2. A high-angle annular dark-field scanning transmission electron microscopy (HAADF–STEM) image and the corresponding energy-dispersive X-ray (EDX) mapping (Figure 3c) showed that the Mo and O atoms were distributed homogeneously.

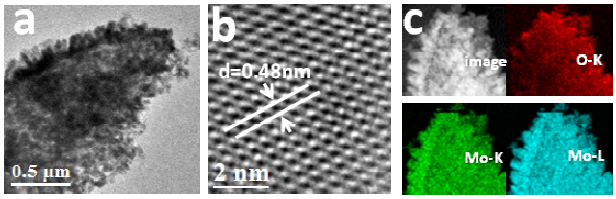

Fig. 3. a) TEM image and b) HRTEM image of MoO_2 and c) STEM image and the corresponding EDX elemental mapping images of O and Mo for MoO_2.

Figure 4a shows the steady-state potential polarization curves of Ni foam, commercial 46.7% Pt/C (TKK, Japan, loading: 0.2 mg cm^{-2}) and NFL MoO_2/NF (MoO_2 loading: ~4.5 mg cm^{-2}) in N_2-saturated 1M KOH solution at 25 °C. In sharp contrast, NFL MoO_2/NF is significantly active for the HER with onset overpotential of almost 0V, and additional negative potential leads to rapid increase in the cathodic current. This value is superior to most of reported values for non-precious-metal HER electrocatalysts (Table S1, Supporting Informatioon). In addition, NFL MoO_2/NF needs overpotentials of only about 55 and 80 mV to achieve current densities of 10 and 20 mA cm^{-2}, respectively. The inset picture in Figure 4a shows the bubbles on NFL MoO_2/NF after steady-state overpotential of only 10 mV for several minutes and Movie S1 shows a HER movie on NFL MoO_2/NF under steady-state overpotential of only 10 mV and 50 mV. Both of them show bubbles produced on the surface of NFL MoO_2/NF under steady-static overpotentials, indicating the onset potential is smaller than 10 mV. The Tafel slopes were 29 mV/dec, 66 mV/dec and 117 mV/dec for commercial 46.7% Pt/C, NFL MoO_2/NF and Ni foam, respectively (Figure 4b). The Tafel slope for NFL MoO_2/NF indicated that the HER proceeds by a Volmer–Heyrovsky mechanism.[28] By using the extrapolation method on the Tafel plots, the exchange current density (j_o) of NFL MoO_2/NF was calculated to be 1.8 mA cm^{-2}.

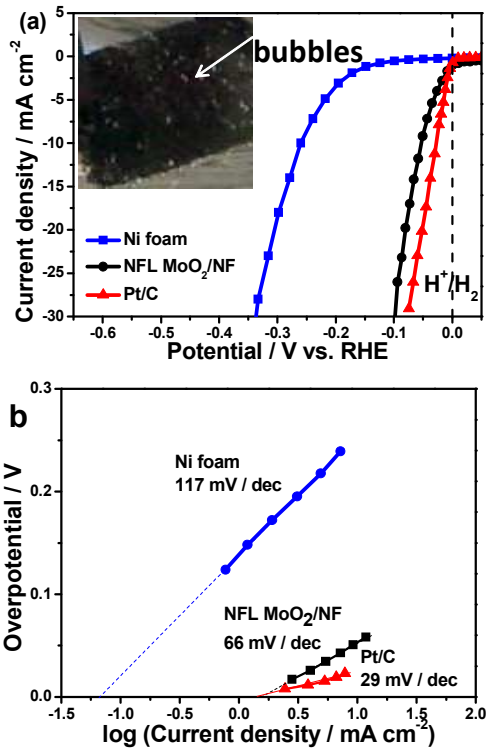

Fig. 4. a) Steady-state polarization curves for Ni foam, NFL MoO_2/NF and commercial Pt/C in 1M KOH. The inset picture in Figure 4a shows the hydrogen bubbles on NFL MoO_2/NF under steady-state potential of only 10 mV for several minutes. b) Tafel plots for Ni foam, NFL MoO_2/NF and commercial Pt/C in 1M KOH.

Furthermore, electrochemical impedance spectroscopy (EIS) experiments were carried out to study the electrode kinetics of the HER. Figure S7, Supporting Informatioon shows the Nyquist plots of the impedance of different catalysts at different overpotentials. The absence of Warburg impedance indicates that the reaction is kinetically controlled, while the presence of only one semicircle in each Nyquist plot reveals

that the equivalent circuit for the HER is characterized by one time constant.[29] Thus, as shown in the inset of Figure S7a, the HER can be described by a simple equivalent electrical circuit, the solution resistance *Rs* is approximately 1.1 Ω for both electrodes. With respect to *Rct*, there is a very large difference between the two electrodes. For instance, at η=100 mV, *Rct* is only 2.4 Ω for the NFL MoO_2/NF electrode remarkably smaller than that for Ni foam (~80 Ω). The *Rct* value is strongly related to the kinetics of the HER. The lower the *Rct* value, the more active the associated electrode for the catalytic reaction.[30] Therefore, it is clear that the NFL MoO_2/NF electrode is more active for the catalysis of HER than that of Ni foam electrode. Figure S8, Supporting Informatioon shows the polarization curve of NFL MoO_2/NF in 1M KOH at different temperatures. The HER activation energy on NFL MoO_2/NF is about 20.0 kJ mol^{-1}, according to the Arrhenius Equation and Arrhenius plots.[31] The activation energy of NFL MoO_2/NF is lower than other none-precious metal catalysts.[32-34]

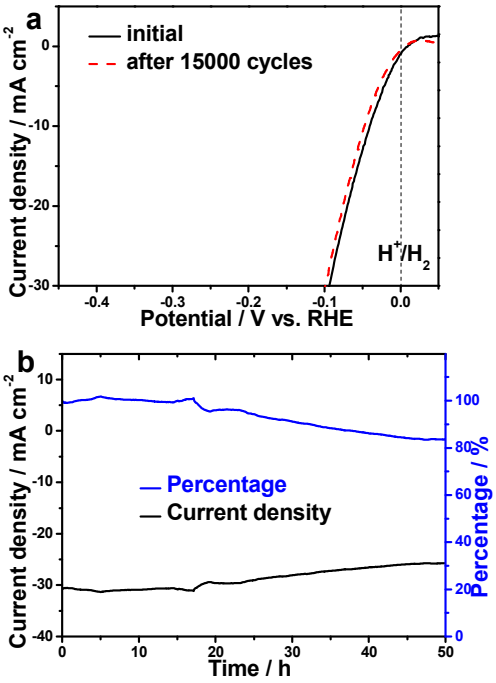

Fig. 5. a) Polarization curves of the NFL MoO_2/NF in 1M KOH initially and after 15,000 CV scanning between +0.05 and -0.15 V *vs*. RHE. b) time-dependent current density curve for NFL MoO_2/NF under steady-state overpotential of 100 mV for 50 h.

The durability of NFL MoO_2/NF was examined. As shown in Figure 5a, the NFL MoO_2/NF exhibited a fairly stable performance within the accelerated degradation measurement for 15,000 cyclic voltammetry (CV) cycles between +0.05 and -0.15 V *vs*. RHE in N_2-saturated 1M KOH at a scan rate of 50 mV s^{-1}. The Figure 5b shows the time dependent current density and percentage curves for NFL MoO_2/NF under steady-state overpotential of 100 mV, NFL MoO_2/NF kept 94.3 and 83.6 percent of its initial current density after 25 and 50 hours, respectively. After a long period of time, the current density only slightly degraded, indicating that the NFL MoO_2/NF has superior stability in the long-term electrochemical process.

The superior HER electrocatalytic performance and stability of the NFL MoO_2/NF could be attributed to the following reasons: 1) MoO_2 possesses good electrical conductivity because it has a distorted rutile structure and its banding involves delocalization of some of the Mo electrons in a conductance band, 2) the nanoflower-like structure of NFL MoO_2/NF could lead to high surface area, there are correspondingly many active sites exposed for HER, 3) NFL MoO_2/NF avoids the use of polymer binder which would block active sites, inhibiting diffusion and increases the time of exposure to air and 4) the porous configuration of Ni foam allows easy diffusion of the electrolyte.

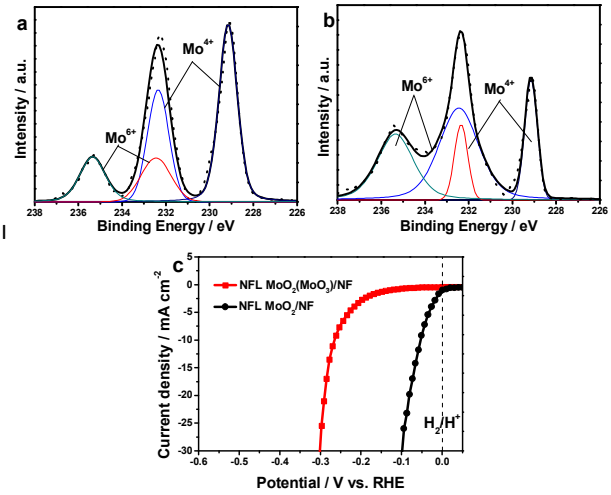

Fig. 6. XPS spectra of Mo 3d for (a) NFL MoO_2/NF and (b) NFL $MoO_2(MoO_3)$/NF. c) The polarization curves of NFL MoO_2/NF and NFL $MoO_2(MoO_3)$/NF in 1M KOH.

t is important to note that the annealing treatment at 400 °C in H_2 atmosphere is indispensable. With an annealing treatment at 500 °C in N_2 atmosphere, the $MoO_2 \cdot 2H_2O$ precursor became MoO_2 (Figure S5) and the surface of MoO_2 was further oxidized into MoO_3 (Figure 6b) due to the remains of oxygen in the tube furnace (NFL $MoO_2(MoO_3)$/NF). A subsequent annealing treatment at 400 °C in H_2 atmosphere was used to reduce the MoO_3 surface of NFL $MoO_2(MoO_3)$/NF to MoO_2 (NFL MoO_2/NF). Figure 6a,b show the X-ray photoelectron spectroscopy (XPS) spectra of Mo 3d for NFL $MoO_2(MoO_3)$/NF and NFL MoO_2/NF, the Mo $3d_{5/2}$ peak of Mo^{6+} was almost coincident with the Mo $3d_{3/2}$ peak of Mo^{4+}, thus leading to the characteristic three-peak shape of Mo^{6+} and Mo^{4+}. Treatment at 400 °C in H_2 atmosphere decreased the amount of Mo^{6+} at the surface of MoO_2 and the ratio of O/Mo from 2.215 for NFL $MoO_2(MoO_3)$/NF to 2.077 for NFL MoO_2/NF.

Figure 6c shows the steady-state polarization curves of NFL MoO_2/NF and NFL $MoO_2(MoO_3)$/NF in N_2-saturated 1M KOH solution at 25 °C. In sharp contrast, NFL $MoO_2(MoO_3)$/NF is less active for the HER with onset overpotential of about

150mV. In addition, NFL MoO_2/NF needs overpotentials of only about 55 mV to achieve current densities of 10 mA cm^{-2}, however, NFL $MoO_2(MoO_3)$/NF needs overpotentials of about 265 mV to achieve current densities of 10 mA cm^{-2}. The bad HER performance of NFL $MoO_2(MoO_3)$/NF could be attributed to the MoO_3 surface, which blocked MoO_2 from contacting with electrolyte. MoO_3 dissolves in alkaline solution and MoO_2 does not dissolve in alkaline solution. Thus, MoO_2 can be stored in alkaline solution and the MoO_3 surface would dissolve and the MoO_2 would reveal again.

Figure 6a and Figure S9, Supporting Informatioon show the X-ray photoelectron spectroscopy (XPS) data in the Mo 3d and O 1s regions for NFL MoO_2/NF, respectively. It is known that peaks at ~ 530 eV are due to oxides and the one at ~ 532 eV is attributed to adsorbed oxygen. Two peaks at 232.4 and 229.2 eV in the Mo 3d region and peaks at ~530.0 eV in the O 1s region are close to the binding energies for Mo and O in MoO_2. The Mo $3d_{3/2}$ binding energy of 232.4 eV is positively shifted from that of metallic Mo $3d_{3/2}$ (231.0 eV) and the Mo $3d_{5/2}$ binding energy of 229.2 eV is positively shifted from that of metallic Mo $3d_{5/2}$ (228.0 eV).[35, 36] While the O 1s has a lower binding energy (~530.0 eV) than oxygen (~532 eV). It suggests that the Mo has a partial positive charge (δ^+) but the O has a partial negative charge (δ^-), thus implying the transfer of electrons from Mo to O.[37-39] A metal complex HER catalyst incorporates proton relays from pendant acid or basic groups, positioned close to the metal center where hydrogen production occurs.[40, 41] Recent work showed that MoP, CoP and FeP as highly active HER catalysts consist of the metal center (δ^+) and the pendant base P (δ^-) close to it.[37-39] Given that MoO_2 is also rich with metal centers (Mo; δ^+) and pendant bases (O; δ^-) positioned close to it, it is believed that it adopts a catalytic mechanism similar to that of metal complex, like MoP, CoP and FeP catalysts for the HER. The Mo and basic O act as the hydride-acceptor and proton-acceptor center, respectively, thus facilitating the HER.[42]

To probe the morphology and composition of the NFL MoO_2/NF after HER electrocatalysis, the SEM, XRD and XPS results of a post-HER NFL MoO_2/NF were collected. As shown in Figure S10-S11, nanoflower-like morphology is preserved and the composition is still MoO_2. Figure S12 shows the X-ray photoelectron spectroscopy (XPS) spectrum of Mo 3d for NFL MoO_2/NF after HER electrolysis, the amount of Mo^{6+} was decreased due to MoO_3 dissolves in alkaline solution.

Conclusions

In conclusion, nanoflower-like MoO_2 has been synthesized successfully for the first time according to our self-developed method. NFL MoO_2/NF showed excellent HER electrocatalytic performance and durability in alkaline electrolytes. The onset potential of NFL MoO_2/NF is almost 0V versus RHE and bubbles can be seen on the surface under steady-state overpotential of only 10 mV. NFL MoO_2/NF needs overpotentials of only about 55 and 80 mV to achieve current densities of 10 and 20 mA cm^{-2}, respectively.

.

Acknowledgements

This work was supported by the Major International (Regional) Joint Research Project (51210002), the National Basic Research Program of China (2015CB932304) and the Specialized Research Fund for the Doctoral Program of Higher Education of China (20110171110024). PKS acknowledge the support from the Danish project of Initiative toward Non-precious Metal Polymer Fuel Cells (4106-000012B).

Notes and references

1 E. David, *Journal of Materials Processing Technology,* 2005, **162,** 169-177.
2 J. D. Holladay, J. Hu, D. L. King and Y. Wang, *Catalysis Today,* 2009, **139,** 244-260.
3 K. Zeng and D. Zhang, *Fuel,* 2014, **116,** 692-698.
4 Y. Sun, M. Delucchi and J. Ogden, *International Journal of Hydrogen Energy,* 2011, **36,** 11116-11127.
5 Y. Li, H. Zhang, T. Xu, Z. Lu, X. Wu, P. Wan, X. Sun and L. Jiang, *Advanced Functional Materials,* 2015, **25,** 1737-1744.
6 Y. Wang, G. Zhang, W. Xu, P. Wan, Z. Lu, Y. Li and X. Sun, *ChemElectroChem,* 2014, **1,** 1138-1144.
7 H. Zhang, Y. Li, G. Zhang, T. Xu, P. Wan and X. Sun, *Journal of Materials Chemistry A,* 2015, **3,** 6306-6310.
8 D. Kong, H. Wang, J. J. Cha, M. Pasta, K. J. Koski, J. Yao and Y. Cui, *Nano Letters,* 2013, **13,** 1341-1347.
9 M. A. Lukowski, A. S. Daniel, F. Meng, A. Forticaux, L. Li and S. Jin, *Journal of the American Chemical Society,* 2013, **135,** 10274-10277.
10 Y. Li, H. Wang, L. Xie, Y. Liang, G. Hong and H. Dai, *Journal of the American Chemical Society,* 2011, **133,** 7296-7299.
11 W. Cui, C. Ge, Z. Xing, A. M. Asiri and X. Sun, *Electrochimica Acta,* 2014, **137,** 504-510.
12 Z. Pu, Q. Liu, A. M. Asiri, Y. Luo, X. Sun and Y. He, *Electrochimica Acta,* 2015, **168,** 133-138.
13 H. Wang, D. Kong, P. Johanes, J. J. Cha, G. Zheng, K. Yan, N. Liu and Y. Cui, *Nano Letters,* 2013, **13,** 3426-3433.
14 H. Vrubel and X. Hu, *Angewandte Chemie-International Edition,* 2012, **51,** 12703-12706.
15 C. Wan, Y. N. Regmi and B. M. Leonard, *Angewandte Chemie-International Edition,* 2014, **53,** 6407-6410.
16 W. F. Chen, C. H. Wang, K. Sasaki, N. Marinkovic, W. Xu, J. T. Muckerman, Y. Zhu and R. R. Adzic, *Energ Environ Sci,* 2013, **6,** 943-951.
17 W. Cui, N. Cheng, Q. Liu, C. Ge, A. M. Asiri and X. Sun, *ACS Catalysis,* 2014, **4,** 2658-2661.
18 C. Ge, P. Jiang, W. Cui, Z. Pu, Z. Xing, A. M. Asiri, A. Y. Obaid, X. Sun and J. Tian, *Electrochimica Acta,* 2014, **134,** 182-186.
19 J. Kibsgaard and T. F. Jaramillo, *Angewandte Chemie-International Edition,* 2014, **53,** 14433-14437.
20 W. Cui, Q. Liu, Z. Xing, A. M. Asiri, K. A. Alamry and X. Sun, *Applied Catalysis B: Environmental,* 2015, **164,** 144-150.
21 V. Eyert, R. Horny, K. H. Hock and S. Horn, Journal of Physics-Condensed Matter, 2000, ***12,*** 4923-4946.
22 R. Wu, J. Zhang, Y. Shi, D. Liu and B. Zhang, *Journal of the American Chemical Society,* 2015, **137,** 6983-6986.
23 S. Cheng, H. Liu and B. E. Logan, *Environmental Science & Technology,* 2006, **40,** 364-369.
24 G. Sasikumar, J. W. Ihm and H. Ryu, *Electrochimica Acta,* 2004, **50,** 601-605.
25 J. Tian, Q. Liu, N. Cheng, A. M. Asiri and X. Sun, *Angewandte Chemie-International Edition,* 2014, **53,** 9577-9581.
26 M. Dieterle and G. Mestl, *Physical Chemistry Chemical Physics,* 2002, **4,** 822-826.

27 Y. Liang, Z. Yi, S. Yang, L. Zhou, J. Sun and Y. Zhou, *Solid State Ionics,* 2006, **177,** 501–505.
28 S. A. Vilekar, I. Fishtik and R. Datta, *Journal of the Electrochemical Society,* 2010, **157,** B1040-B1050.
29 D. Merki, H. Vrubel, L. Rovelli, S. Fierro and X. Hu, *Chemical Science,* 2012, **3,** 2515-2525.
30 N. Krstajić, M. Popović, B. Grgur, M. Vojnović and D. Šepa, *Journal of Electroanalytical Chemistry,* 2001, **512,** 16–26.
31 K. J. Laidler, *Journal of Chemical Education,* 1984, 61, 494.
32 I. A. Raj and K. Vasu, *Journal of Applied Electrochemistry,* 1992, **22,** 471-477.
33 A. B. Papandrew and T. A. Zawodzinski, *Journal of Power Sources,* 2014, **245,** 171-174.
34 M. De Giz, M. Ferreira, G. Tremiliosi-Filho and E. Gonzalez, *Journal of Applied Electrochemistry,* 1993, **23,** 641-645.
35 E. Minni and F. Werfel, *Surface & Interface Analysis,* 1988, **12,** 385–390.
36 B. Brox, I. Olefjord, *Surface & Interface Analysis,* 1988, **13,** 3-6.
37 Z. Xing, Q. Liu, A. M. Asiri and X. Sun, *Advanced Materials,* 2014, **26,** 5702-5707.
38 J. Tian, Q. Liu, A. M. Asiri and X. Sun, *Journal of the American Chemical Society,* 2014, **136,** 7587-7590.
39 P. Jiang, Q. Liu, Y. Liang, J. Tian, A. M. Asiri and X. Sun, *Angewandte Chemie-International Edition,* 2014, **126,** 13069–13073.
40 R. H. Newell, D. L. Dubois, A. D. Wilson, M. R. Dubois, M. J. Mcnevin and J. T. Muckerman, *Journal of the American Chemical Society Jacs,* 2006, **128,** 358-366.
41 B. E. Barton and T. B. Rauchfuss, *Journal of the American Chemical Society,* 2010, **132,** 14877-14885.
42 J. A. Rodriguez, *Journal of the American Chemical Society,* 2005, **127,** 14871-14878.